Earth return admittance and frequency-dependent soil parameters effect on transient behavior of the earth continuity conductor

J. E. Guevara Asorza, R.A. de Araujo, J. Pissolato Filho

***Abstract*—The Earth Continuity Conductor (ECC) is required in underground transmission systems that utilize single-point bonding or cross-bonding. Proper electrical design of these systems requires thoroughly analyzing the ECC's steady-state and transient behavior. This paper focuses on the influence of earth-return admittance, earth displacement current, and frequency-dependent soil parameters on the transient behavior and lightning response of the ECC. The results highlight significant differences in the ECC's performance when these factors are considered, particularly regarding overvoltages in the conductor and the energy capacity of the sheath voltage limiter (SVL), a device commonly used in single-point bonding configurations.**

***Keywords*—Earth-return admittance, earth continuity conductor, electromagnetic transients, frequency-dependent soil, underground transmission lines**

I. Introduction

THE rapid growth of urban areas in recent decades has rendered the exclusive use of overhead transmission lines (OHTLs) for interconnecting power substations increasingly unfeasible, primarily due to space constraints that limit the installation of transmission towers. In this context, underground transmission lines (UGTL) are necessary, especially for sections entering urban areas. In some cases, these sections are relatively short, making the cross-bonding (CB) method economically impractical. Consequently, single-point bonding (SPB) is adopted, requiring an earth continuity conductor (ECC) to handle ground fault currents and the associated rise in ground potential [1], [2]. In the literature, the design of the ECC under steady-state conditions and its associated issues are well-discussed [3]–[5]. However, few studies focused on the transient behavior of UGTL with ECC in SPB configurations [6]. Most studies concentrate on UGTL systems with CB configurations. Transient analysis of these systems requires accurate UGTL modeling, including calculating series impedance and shunt admittance. Traditionally, the Pollaczek formulation [7] is employed to estimate the earth-return impedance, with the infinite complex integrals resolved through various mathematical methods [8], [9]. However, this formulation neglects the earth-return admittance and the soil permittivity, which significantly impact the frequency range of tens of kHz [10]. Thus, Papadopoulos [10] and Xue [11] proposed a extended transmission line (TL) approach to calculate the earth-return impedance and admittance to address these limitations based on a solution of Maxwell's equations, considering different Hertizian vectors. Closed forms for computing the extended TL approach from Xue were developed, such as the one carried by De Conti [12], using asymptotic approximations and leveraging the rapid decay of the exponential function. In [13], a transient response analysis was carried out comparing the extended TL approaches proposed by Papadopoulos and Xue with a full-wave model based on the finite-difference time-domain (FDTD) method, where both extended TL formulations exhibit equivalent accuracy in reproducing the transient behavior. Additionally, extended TL approach by Xue has been validated through field tests [14] and the MoM-So method [11]. Additionally, the inclusion of frequency-dependent soil parameters in UGTL systems has been investigated in [15], [16], focusing on systems with CB configurations. On the other hand, in works such as [17], [18] presented lightning analysis in mixed transmission lines, focusing in lightning performance and not in the cable modeling. In this context, the main contribution of this work is to evaluate the impact of earth-return admittance and frequency-dependent soil parameters on the calculation of electrical parameters, transient behavior, and lightning response of UGTL systems with SPB, which includes the ECC. Furthermore, it investigates how the ECC influences propagation modes in UGTL systems.

This paper was supported by the São Paulo Research Foundation (FAPESP) grants: 2021/11258-5, 2023/05066-1 and 2024/14472-6. J. E. Guevara Asorza is with the University of Campinas - UNICAMP, Campinas, Brazil, (e-mail of corresponding author: j272296@dac.unicamp.br). R. A. Araujo is with the Federal University of Lavras (UFLA), Brazil (e-mail: ricardo.araujo@ufla.br). J. P. Filho is with the University of Campinas - UNICAMP, Campinas, Brazil, (e-mail: pisso@unicamp.br).

Paper submitted to the International Conference on Power Systems Transients (IPST2025) in Guadalajara, Mexico, June 8-12, 2025.

II. Classical and Extended TL approach

In the literature, there are two transmission line approaches for calculating earth-return parameters [11]: the classical approach, based on Pollaczek's formulations, and the extended approach, which for this study, the Xue's formulas are used. The main difference between these approaches lies in treating earth-return impedance, earth-return admittance, and the consideration of the relative permittivity of the soil (ϵ_r). Meanwhile, the internal impedance (of the core and insulation layer) and the insulation admittance are identical in both approaches, as described in [19]. The earth-return impedance and admittance for the extended TL approach can be determined as follows, considering the physical positioning of two cables in the soil (position i and j).

$$Z_{g(i,j)} = \frac{jw\mu_0}{2\pi}\left[\Lambda + \Delta_4^{QT} + \gamma_1^2\Delta_6^{QT}\right] \quad (1)$$

$$P_{g(i,j)} = \frac{jw\mu_0}{2\pi(\sigma_1 + jw\varepsilon_1)}\left[\Lambda + \Delta_5^{QT} + \gamma_1^2\Delta_6^{QT}\right] \quad (2)$$

$$\Lambda = K_0(\gamma_1 d_{ij}) - K_0(\gamma_1 D_{ij}) \quad (3)$$

$$\Delta_4^{QT} = 2\int_0^\infty \left[\frac{e^{-(h_i+h_j)u_1}}{u_0+u_1}\right]\frac{\lambda^2}{u_1^2}cos(x\lambda)d\lambda \quad (4)$$

$$\Delta_6^{QT} = 2\int_0^\infty \left[\frac{e^{-(h_i+h_j)u_1}}{u_0+u_1}\right]\frac{1}{u_1^2}cos(x\lambda)d\lambda \quad (5)$$

$$u_0 = \sqrt{\lambda^2+\gamma_0^2},\ \ u_1 = \sqrt{\lambda^2+\gamma_1^2} \quad (6)$$

$$\gamma_0 = jw\sqrt{\mu_0\varepsilon_0},\ \ \gamma_1 = \sqrt{jw\mu_0(\sigma_1+jw\varepsilon_1)} \quad (7)$$

$$d_{ij} = \sqrt{(h_i-h_j)^2+x^2},\ \ D_{ij} = \sqrt{(h_i+h_j)^2+x^2} \quad (8)$$

$$\Delta_5^{QT} = 2\int_0^\infty \left[\frac{e^{-(h_i+h_j)u_1}}{u_0+\gamma_0^2\gamma_1^{-2}u_1}\right]\frac{\lambda^2}{u_1^2}cos(x\lambda)d\lambda \quad (9)$$

$$\Delta_6^{QT} = 2\int_0^\infty \left[\frac{e^{-(h_i+h_j)u_1}}{u_0+u_1}\right]\frac{1}{u_1^2}cos(x\lambda)d\lambda \quad (10)$$

where K_0 is the modified Bessel function of the second kind with order zero, γ_0 is the propagation constant of the air, γ_1 is the propagation constant of the ground, μ_0 is the vacuum permeability, μ_1 is the ground permeability which is the same of the vacuum permeability, ε_0 is the permittivity of the air, ε_1 is the permittivity of the ground, σ_1 is the ground conductivity. Furthermore, h_i and h_j are the depth installation of the cables i and j, and x is the horizontal distance between the cables i and j. For calculating the self-earth-return impedance matrix, it is possible to consider $h_i = h_j$ and x as the external radius of the cable. The earth-return admittance is calculated by doing the inverse of the potential coefficients matrix, P_g.

III. Frequency-dependent soil parameters

From an electrical perspective, soil can be characterized by its conductivity (σ_g), dielectric permittivity (ε_r), and magnetic permeability (μ), with the latter assumed to be equal to μ_0. Several formulations have been proposed to describe the frequency dependence of these parameters—such as the Alipio-Visacro model [20] and the Longmire and Smith (LS) model [21]—and are thoroughly discussed in the literature [22]–[24]. According to [25], both σ_g and ε_r are significantly influenced by frequency. This is due to various phenomena that occur within the frequency range of lightning currents, such as electronic polarization, ionic polarization, conduction, and loss mechanisms. This study considers the frequency-dependent behavior of soil's electrical parameters using the model recommended by CIGRE 781, given by:

$$\rho_g(f) = \rho_0\left\{1 + 4.7\cdot 10^{-6}\cdot\rho_0^{0.73}\cdot f^{0.54}\right\}^{-1} \quad (11)$$

$$\varepsilon_r(f) = 12 + 9.5\cdot 10^4\cdot\rho_0^{-0.27}\cdot f^{-0.46} \quad (12)$$

where ρ_0 is the low-frequency soil resistivity in Ω·m, and f is the frequency Hz.

IV. Modal parameters for UGTL

The number of elements that can be energized or induced by others defines the order of the series impedance matrix and the shunt admittance matrix. In this context, since the study focuses on a single-circuit UGTL with ECC, the matrix order will be seven. Modal parameters are used to represent the UGTL in a domain where there is no coupling between the metallic elements. In other words, the goal is to transition from the phase domain to the modal domain. For that purpose, a transformation matrix is required, which is calculated using the series impedance matrix (Z) and the shunt admittance matrix (Y), for each frequency value. Based on the theory of eigenvalues and eigenvectors, it is possible to decouple the product of the Z and Y matrices into a diagonal matrix [26].

$$D = T_i^{-1}.Y.Z.T_i \quad (13)$$

where D_i contains the eigenvalues of the matrix product $Y.Z$ and T_i is the matrix of eigenvectors. For calculating the modal matrices, Z_m and Y_m, is necessary to solve the linear system:

$$[Y.Z - D_k I]\,T_{i,k} = 0 \quad (14)$$

where D_k represents the kth eigenvalue of the matrix product, I is the identity matrix and $T_{i,k}$ denotes the kth column of the modal matrix. The solution of this linear system can be solved by different methods such as Newton Raphson (NR) method [27] or Sequential Quadratic Programming (SQP) [28]. In this paper, we considered the Levenberg–Marquardt (LM) algorithm [24], [29], [30] due to its robust convergence, accuracy, and efficiency in this type of problem. Then, the modal matrices Z_m and Y_m are calculated as a function of the matrix transformation T_i, so that later the elements of the diagonal modal propagation matrix (γ_k), which contains the phase velocity (β_k) and the attenuation constant (α_k), are calculated by (15), where k represents the diagonal element.

$$\gamma_k = \alpha_k + j\beta_k = \sqrt{Z_{m,k}Y_{m,k}} \quad (15)$$

V. Results

In this section, the wave propagation characteristics and transient response, by step source of 1 kV and lightning current waveform, are analyzed for a single-circuit UGTL at 220 kV in a triangular configuration, considering the SPB method with the ECC, where its position is at the center of the triangular configuration to avoid ECC transposition [5]. Both classical and extended TL approaches are examined in detail for each analysis, with particular emphasis on the response of the ECC. In addition, the extended approach with frequency-dependent characteristics of the soil was included. The extended approach includes the effect of displacement current and earth-return admittance. For this study, three different soil electrical resistivity values are considered: 100, 1000, and 2500 Ω·m. Table I presents the primary data required for the study. The cable used is a single-core 1600 mm^2 with core, sheath, and XLPE insulation, while the ECC is a single-core 185 mm^2 with XLPE insulation [31].

A. Modal Analysis

Two key variables that describe the wave behavior in the modes are the phase velocity (υ) and the attenuation constant (α).

TABLE I: Input data of the UGTL

Description	Unit	Value
Inner core radius, r_1	mm	0.00
Outer core radius, r_2	mm	24.70
Insulation XLPE radius, r_3	mm	50.10
Sheath radius, r_4	mm	52.68
Outer insulation radius, r_5	mm	57.78
Core resistivity DC a 20 °C, ρ_c	Ω.m	2.16x10^{-8}
Sheath resistivity DC a 20 °C, ρ_s	Ω.m	5.33x10^{-8}
Inner insulation relative permittivity	-	2.75
Outer insulation relative permittivity	-	2.3
Ground relative permittivity, ϵ_{gr1}	-	12
Depth installation at the center of the configuration, h	m	1.502
Separation distance between cables, S	m	0.35
Inner core radius of ECC	mm	0.00
Outer core radius of ECC	mm	8.1
Core resistivity DC a 20 °C of ECC, ρ_{ecc}	Ω.m	1.72x10^{-8}
External radius of ECC	mm	12
Outer insulation relative permittivity of ECC	-	2.3

With the inclusion of the ECC in the triangular duct arrangement, electromagnetic coupling occurs between the phase cable and the ECC, increasing the number of cables in the duct from 3 to 4. Thus, to decouple these cables and analyze the modes, the Levenberg-Marquardt algorithm was used, resulting in four distinct modes: coaxial, intersheath, ground, and ECC mode. The latter alters the natural behavior of the other modes. The propagation characteristics of the mode as a function of frequency, for a soil resistivity of 1000 Ω·m, are presented in Fig. 1.

The solid lines correspond to the classical TL approach based on the Pollaczek formula (P.F), whereas the dashed lines represent the extended TL approach employing the Xue formulation (X.F). Finally, the x-lines indicate the extended TL approach that incorporates the frequency-dependent characteristics of the soil (X.F(f)).

As expected, the coaxial mode shows no difference in phase velocity or attenuation constant between approaches, as these depend solely on the cable's internal properties. Above 10 kHz, the phase velocity remains constant, and all three coaxial modes exhibit similar propagation characteristics due to the triangular arrangement of the single-core cables within the duct. On the other hand, noticeable differences are observed between approaches in the attenuation constant and phase velocity for the intersheath, ground, and ECC modes at high frequencies. The ECC mode has a higher phase velocity than the intersheath and ground modes; however, its attenuation is lower than these modes. In general, accounting for the frequency dependence of soil electrical properties in the extended TL approach reduces the attenuation constant and phase velocity compared to the frequency-independent case across the ground, ECC, and intersheath modes. Significant differences in propagation characteristics—especially for the ground and intersheath modes—between classical and extended approaches have been reported in [11], [32], with the influence of frequency-dependent soil parameters further emphasized in [23].

To provide a physical understanding of each mode, the real part of the eigenvector matrix, T_i, at 1 MHz is presented in (16), when the extended TL approach with frequency-dependent grounding properties is used. Columns 1 to 3 of T_i represent the coaxial mode for each phase, where currents flow exclusively between the cores and the sheaths, with no current flowing into the ECC or the ground. Columns 4 and 5 represent the intersheath mode, where currents flow only into the sheaths without affecting the ECC. Column 6, representing the ground mode, shows currents flowing into the sheaths into the ECC, and finally, in the ECC mode, currents flow into both the sheaths and the ECC. In the literature, studies like [6] present the ECC mode as an intersheath ECC mode because, in the flat configuration used, the ECC is not positioned at the center of the duct bank, allowing currents to flow into the ECC in the intersheath modes. However, in the present study, where a triangular configuration with the ECC centered in the duct bank is considered, no current flows into the ECC when the intersheath modes are analyzed.

$$T_i = \begin{bmatrix} 0.41 & -0.50 & -0.29 & 0 & 0 & 0 & 0 \\ -0.41 & 0.50 & 0.29 & -0.71 & -0.41 & 0.57 & -0.29 \\ 0.41 & -0.01 & 0.58 & 0 & 0 & 0 & 0 \\ -0.41 & 0.01 & -0.58 & 0 & 0.82 & 0.57 & -0.29 \\ 0.41 & 0.5 & -0.29 & 0 & 0 & 0 & 0 \\ -0.41 & -0.5 & 0.29 & 0.71 & -0.41 & 0.57 & -0.29 \\ 0 & 0 & 0 & 0 & 0 & 0.14 & 0.87 \end{bmatrix} \quad (16)$$

Moreover, to quantify the influence of the displacement current and the earth-return admittance, normalized propagation parameter $p_{1_{norm}}$ is analyzed [24], [30], while, for quantify, besides the displacement current and earth-return admittance, the frequency-dependence of the soil electrical characteristics, the normalized propagation $p_{2_{norm}}$ is used. The normalized propagation parameter, $p_{1_{norm}}$, is the ratio between the extended TL and the classic TL approach; while $p_{2_{norm}}$ is the ratio between the extended TL approach with frequency-dependence of the soil electrical characteristics and the classic TL approach, as shown in (17) and (18), respectively.

$$p_{1_{norm}} = \frac{P.characteristics_{Xue}}{P.characteristics_{Pollaczek}} \quad (17)$$

$$p_{2_{norm}} = \frac{P.characteristics_{Xue(f)}}{P.characteristics_{Pollaczek}} \quad (18)$$

The normalized modes, except for the coaxial mode, are presented in Figs. 2 and 3, considering three different values of soil electrical resistivity: 100, 1000, and 2500 Ω·m. The intersheath mode selected in this study is where the current flows through the sheath of all three cables. As the soil electrical resistivity increases, the differences between the modes become more pronounced, especially starting from a few kHz. However, these differences are negligible for frequencies near steady-state conditions. With the extended TL approach, notable differences in the attenuation constant emerge at high frequencies, particularly as soil resistivity increases—most prominently in the intersheath and ECC modes, though still relevant in the ground mode. Incorporating the frequency dependence of soil properties reduces these discrepancies, as resistivity and permittivity decrease with frequency [23], though the deviations remain significant. The most prominent differences in phase velocity occur in the ground mode and grow with higher soil resistivity. These are notably reduced when frequency-dependent parameters are considered—for instance, at ρ = 2500 Ω·m, the phase velocity drops from about six times to 3.6 times the classical TL value.

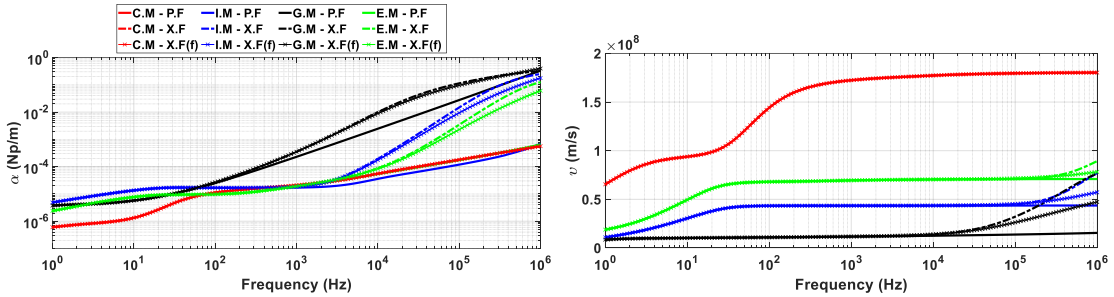

(a) Attenuation constant. (b) Phase velocity.

Fig. 1: Mode propagation characteristics for ρ = 1000 Ω·m.

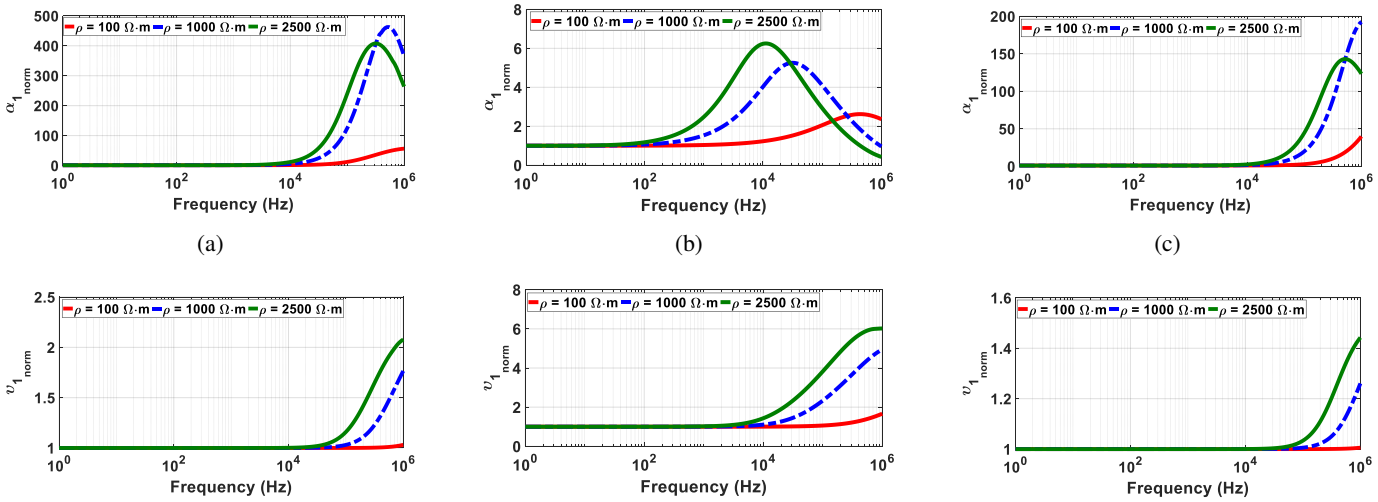

(a) (b) (c)

(d) (e) (f)

Fig. 2: Normalized modes $p_{1_{norm}}$. First row are Attenuation constants and second row are Phase velocity, (a,d) intersheath mode, (b,e) ground mode and (c,f) ECC mode.

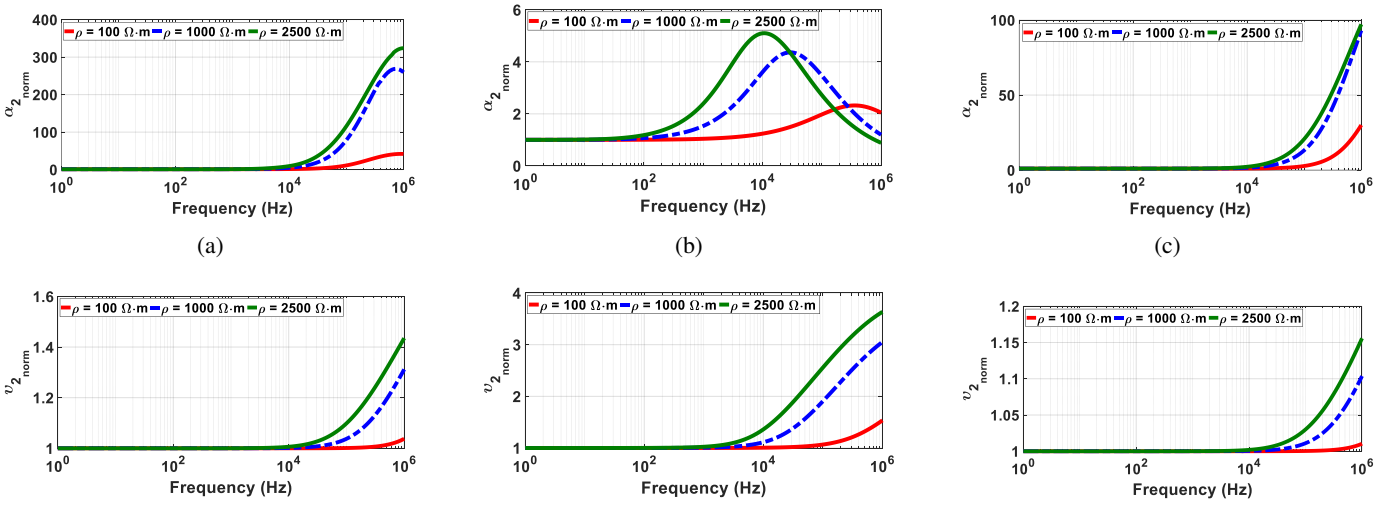

(a) (b) (c)

(d) (e) (f)

Fig. 3: Normalized modes $p_{2_{norm}}$. The first row is Attenuation constants, and the second row is Phase velocity, (a,d) intersheath mode, (b,e) ground mode, and (c,f) ECC mode.

Differences in attenuation are linked to the conductance in the earth-return admittance. Therefore, neglecting the effects of earth-return admittance, the soil relative permittivity, and frequency-dependent soil properties can lead to significant

discrepancies in the propagation characteristics.

B. Transient response

To analyze the discrepancy between TL approaches with different values of soil electrical resistivity, three cable systems were implemented, and their transient response was analyzed through energization by a step voltage source (1 kV). The implemented cable systems correspond to the intersheath, ground, and ECC modes, whose electrical representations are shown in Fig. 4. The cable length, including the ECC, is 600 meters, which is a typical value for smaller-section UGTLs with SPB. These systems were modeled in PSCAD®, taking into account the physical significance of each mode, as analyzed in the eigenvector matrix, T_i.

The analyzed transient response occurs in the sheath of the phase B cable, where the step source injects the signal, as well as in the ECC, both at the receiving end of the system. It is important to note that the ECC will be energized in the ground and ECC modes. However, in the intersheath mode, the induced voltage in the ECC will be zero due to its specific position within the duct bank.

Fig. 5 shows the overvoltages recorded at the receiving end, measured in the sheath of the phase B cable in the test circuit corresponding to the intersheath mode, as the soil electrical resistivity increases. As soil resistivity increases, discrepancies between modeling approaches become more evident. The impact of frequency-dependent soil properties is minimal for low resistivity (e.g., 100 Ω·m). However, incorporating frequency dependence noticeably reduces the attenuation constant at higher resistivities. In contrast, the classical TL approach consistently underestimates attenuation, potentially misleading the analysis by suggesting limited overvoltage damping with varying soil resistivity.

Fig. 6 displays the transient response at the receiving end of the sheath of phase B cable and the ECC when the circuit test utilized pertains to the ground mode. As it was expected, the overvoltages presented low velocity but a high attenuation, as it was shown in Fig. 1. In this case, the difference between the velocities of the TL approaches increases, and consequently, the difference in the attenuation constant also increases. When the soil electrical resistivity is 2500 Ω·m, the transient response in the sheath and ECC is equal to the input signal for the extended TL approaches after 500 μs; in contrast, for the classical TL approach, it will take longer for the response to attenuate and reach the same value as the signal sent by the voltage source. Moreover, the overvoltage calculated with the classical TL approach takes longer to reach the receiving end. As soil resistivity increases, the peak difference of the first overvoltage becomes more significant. When frequency-dependent soil properties are included in the extended TL model, the reduced resistivity and permittivity at high frequencies result in a higher first peak than the model with constant parameters—consistent with the findings in [16]. Finally, Fig. 7 presents the results obtained at the receiver end for the Phase B cable sheath and the ECC, for the ECC mode circuit test. The differences in phase velocity between TL approaches in overall, are minor. However, the attenuation constant for each TL approach shows a significant differences. These differences in attenuation increases as the soil resistivity increases, making it appear from the results that the only voltage wave being attenuated is the one from the extended TL approaches. Similar to the overvoltages calculated in the ground mode, the inclusion of frequency-dependent soil electrical parameters reduces the attenuation constant, with this effect becoming more pronounced as soil resistivity increases.

C. Lightning response

This study considered the transition between OHTL and UGTL at the tower transition, as is shown in Fig. 8. The electrical parameters for the OHTL were calculated using the voltage formulation proposed by Pettersson [33], while the other elements such as insulator string and transition tower were modeled according to [34]. The atmospheric discharge current used was obtained from real measurements at the Morro do Cachimbo (MCS) stations [35], [36], considering the median current parameters of the first stroke, where the maximum peak is 43.3 kA . The rating voltage considered for the sheath voltage limiters (SVL) was 6 kV, with the V-I curve behavior described in [37]. The bonding leads were simulated as inductance, considering the formulas indicated in [2].

Fig. 8 shows that the transition tower, the SVL and ECC are connected to the same grounding system, while the terminations are connected to the transition tower. For this study, this grounding system was modeled as an resistance of 5 Ω. The atmospheric discharge simulates a shielding failure, striking phase A at the transition tower and propagating in five directions: toward the OHTL behind the tower, the grounding system, the power cable cores, the sheaths, and the ECC. The surge arrester blocks overvoltages entering the cores, while the flow into the sheaths occurs only if the SVL's operating threshold is exceeded. The overvoltage on the ECC adopts the potential of the grounding system. Evaluating this is crucial to prevent insulation degradation.

Fig. 9 shows the overvoltage measured at the receiver end of the ECC when the atmospheric discharge hits phase A (shielding failure) at the tower. Since the ECC is connected to the tower's grounding system, an overvoltage will flow into it. When the classic TL approach is used, there is no significant difference in the overvoltage as the soil's electrical resistivity increases, although a slight decrease occurs. When the classical TL approach is employed, higher overvoltages are observed. In contrast, the extended TL approach reduces nearly 50% in the peak value for a soil resistivity of ρ = 2500 Ω·m. When the frequency dependence of the soil parameters is incorporated into the extended TL model, a slight increase in the peak value is observed compared to the extended TL approach with frequency-independent parameters. Moreover, both extended TL models yield a faster attenuation of the overvoltage waveform than the classical TL approach.

In the same way, Fig. 10 presents the Energy Capability (E.C) of the SVL from phase A, installed in the transition tower, where it is easy to note that as long as the soil electrical resistivity increases, the E.C required decreased. However, this decrease is more notorious when the extended TL approach is used. These differences in energy are primarily attributed to the higher attenuation introduced by the extended TL approaches.

(a) Intersheath mode. (b) Ground mode. (c) ECC mode.

Fig. 4: Cable systems for transient response.

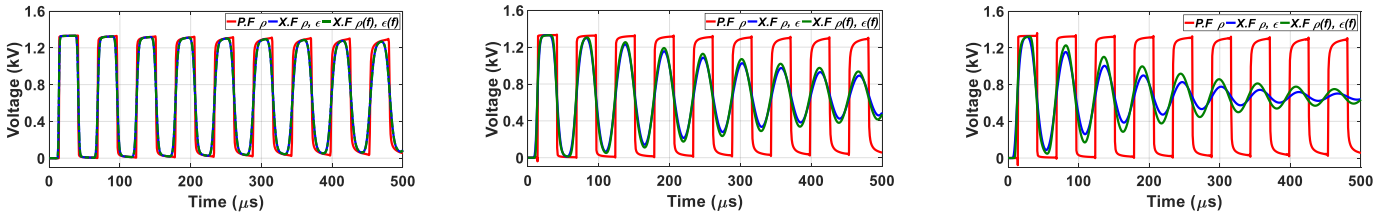

(a) (b) (c)

Fig. 5: Intersheath mode: Transient response at the receiving end for cable sheath from phase B (a) 100 Ω·m (b) 1000 Ω·m, (c) 2500 Ω·m.

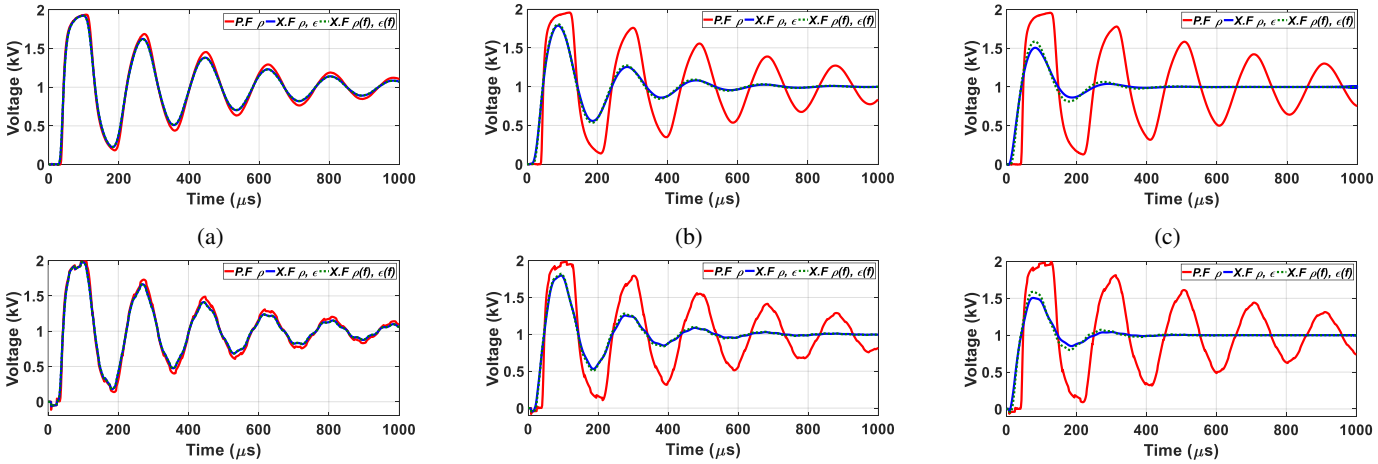

(a) (b) (c) (d) (e) (f)

Fig. 6: Ground mode: Transient response at the receiving end (a) 100 Ω·m - Phase B (b) 1000 Ω·m - Phase B, (c) 2500 Ω·m - Phase B (d) 100 Ω·m - ECC, (e) 1000 Ω·m - ECC, (f) 2500 Ω·m - ECC.

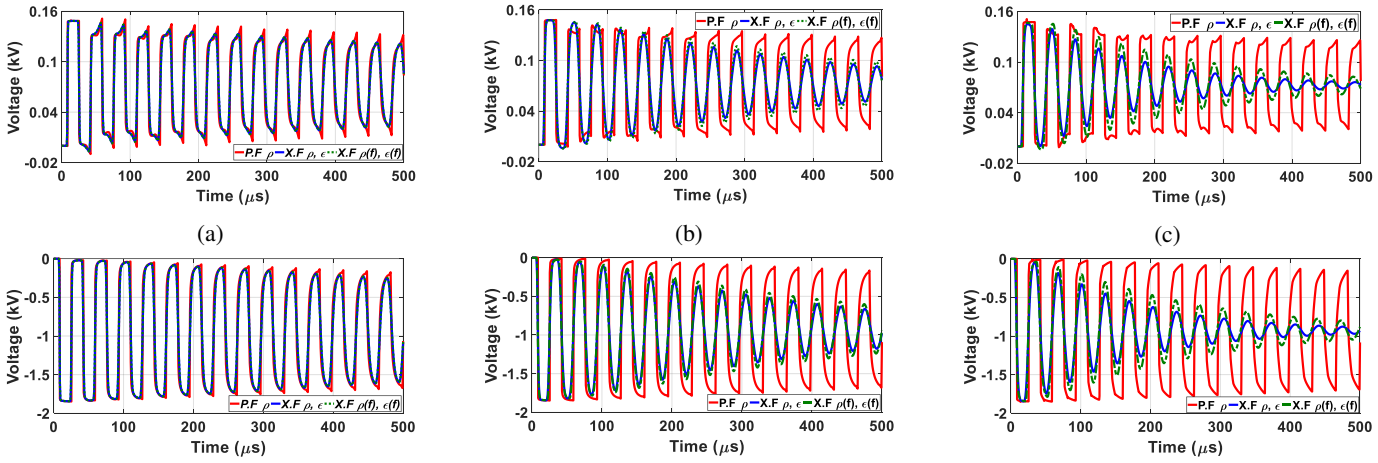

(a) (b) (c) (d) (e) (f)

Fig. 7: ECC mode: Transient response at the receiving end (a) 100 Ω·m - Phase B (b) 1000 Ω·m - Phase B, (c) 2500 Ω·m - Phase B (d) 100 Ω·m - ECC, (e) 1000 Ω·m - ECC, (f) 2500 Ω·m - ECC.

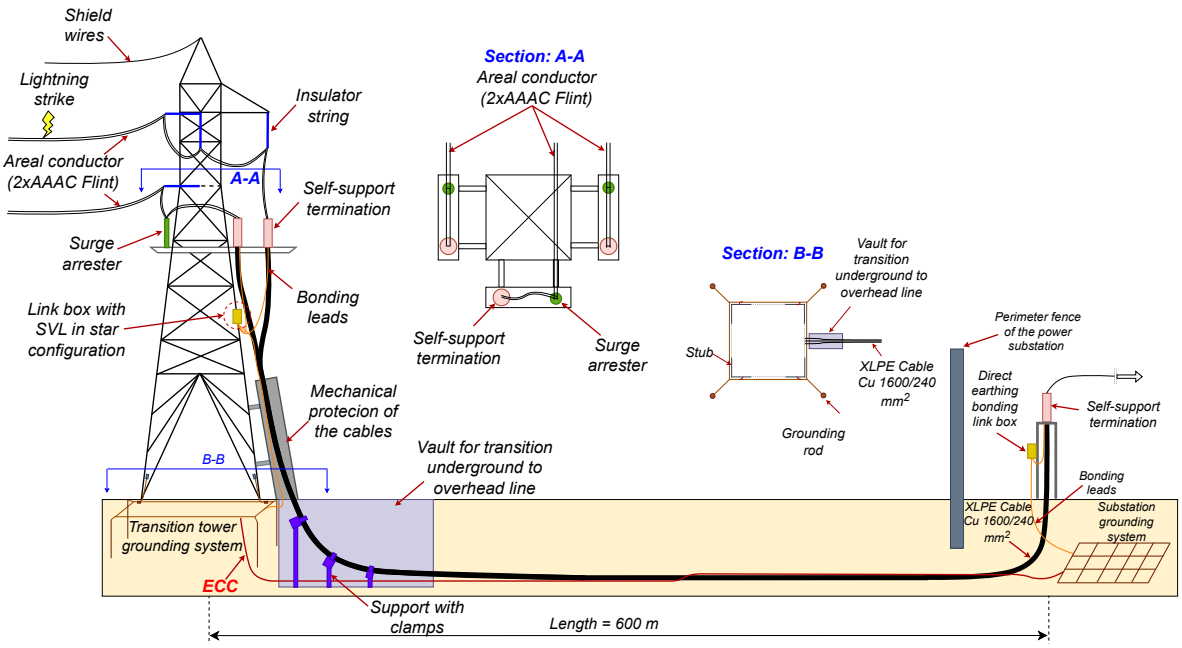

Fig. 8: System under analysis - Transition overhead to underground line.

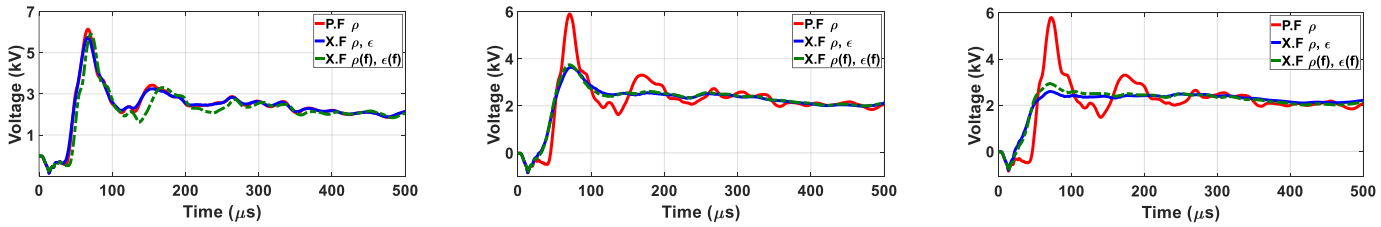

(a) (b) (c)

Fig. 9: Lightning response at receiving end of ECC, (a) 100 Ω·m, (b) 1000 Ω·m and (c) 2500 Ω·m.

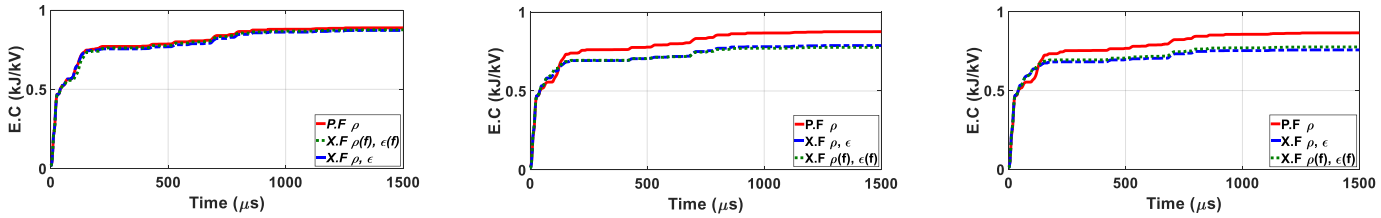

(a) (b) (c)

Fig. 10: Energy capacity of the SVL from the phase A (a) 100 Ω·m, (b) 1000 Ω·m and (c) 2500 Ω·m.

Consequently, relying on the classical TL model may result in overestimating the energy absorbed by SVLs, potentially leading to their oversizing.

VI. Conclusions

This article provides a comprehensive analysis of the transient response in the ECC, focusing on the impact of earth-return admittance parameters and soil frequency dependency. The extended TL approach, which integrates earth-return admittance and soil permittivity, was employed to achieve this. Furthermore, the influence of the frequency-dependence of soil characteristics according to the CIGRE model was incorporate in the extended TL approach. The results were compared and critically evaluated against those obtained using the classical TL model, highlighting key differences and implications. Thus, a modal analysis was conducted to understand how the ECC impacts the power cable core and sheath. The results indicate that the ECC does not interfere with the coaxial and intersheath modes but significantly affects the grounding mode. An ECC mode was also identified, which was associated with the cable sheaths. Although the ECC mode does not alter the physical interpretation of the intersheath mode due to its central position in the triangular duct bank configuration, changes could occur if the ECC were installed in a different position.

Moreover, the results reveal significant differences between the classical and extended TL approaches, particularly at high frequencies, in both phase velocity and attenuation constant. These discrepancies increase with higher soil electrical resistivity. These differences have a direct impact on the transient and lightning response, leading to lower overvoltages at the receiving end of the ECC when either of the extended TL approaches is used—whether with frequency-dependent or constant soil parameters. Furthermore, significant differences were also observed in the energy capability of the SVL. These differences are attributed to the higher attenuation exhibited by the extended TL approaches.

VII. References

[1] I. C. Comittee, "IEEE guide for bonding shields and sheaths of single-conductor power cables rated 5 kV through 500 kV, std. 575," 2014.

[2] CIGRE WG B1.50, "Sheath bonding systems of AC tranmsission cables – Design, testing, and maintenance," 2020, Technical Brochure 797.

[3] J.-B. Lee and C.-K. Jung, "Technical review on parallel ground continuity conductor of underground cable systems," Journal of International Council on Electrical Engineering, vol. 2, no. 3, pp. 250–256, 2012.

[4] M. Li, C. Zhou, W. Zhou, J. Zhang, L. Zhang, and L. Yao, "Feasibility study on lengthening the high-voltage cable section and reducing the number of cable joints via alternative bonding methods," High Voltage, vol. 4, no. 4, pp. 292–299, 2019.

[5] J. E. G. Asorza, J. S. Colqui, F. F. da Silva, and J. P. Filho, "Earth continuity conductor location in single-circuit underground transmission line using the generalized model," Electric Power Systems Research, vol. 235, p. 110879, 2024.

[6] C. F. Jensen, U. S. Gudmundsdottir, C. L. Bak, and A. Abur, "Field test and theoretical analysis of electromagnetic pulse propagation velocity on crossbonded cable systems," IEEE Transactions on Power Delivery, vol. 29, no. 3, pp. 1028–1035, 2014.

[7] F. Pollaczek, "Uber das feld einer unendlich langen wechselstromdurch-flossen einfachleitung," ENT, vol. 3, no. 9, pp. 339–360, 1926.

[8] T. Theodoulidis, "Exact solution of pollaczek's integral for evaluation of earth-return impedance for underground conductors," IEEE Transactions on Electromagnetic Compatibility, vol. 54, no. 4, pp. 806–814, 2012.

[9] F. Uribe, O. Ramos-Leaños, and P. Zuniga, "An investigation of earth and sea-return impedances of power electrical cables," Electric Power Systems Research, vol. 223, p. 109608, 2023.

[10] T. A. Papadopoulos, D. A. Tsiamitros, and G. K. Papagiannis, "Impedances and admittances of underground cables for the homogeneous earth case," IEEE Transactions on Power Delivery, vol. 25, no. 2, pp. 961–969, 2010.

[11] H. Xue, A. Ametani, J. Mahseredjian, and I. Kocar, "Generalized formulation of earth-return impedance/admittance and surge analysis on underground cables," IEEE Transactions on Power Delivery, vol. 33, no. 6, pp. 2654–2663, 2018.

[12] A. De Conti, N. Duarte, and R. Alipio, "Closed-form expressions for the calculation of the ground-return impedance and admittance of underground cables," IEEE Transactions on Power Delivery, vol. 38, no. 4, pp. 2891–2900, 2023.

[13] N. Duarte, A. De Conti, and R. Alipio, "Assessment of ground-return impedance and admittance equations for the transient analysis of underground cables using a full-wave fdtd method," IEEE Transactions on Power Delivery, vol. 37, no. 5, pp. 3582–3589, 2022.

[14] R. Alipio, N. Duarte, and F. Rachidi, "High-frequency transients in buried insulated wires: Transmission line simulations and experimental validation," Electric Power Systems Research, vol. 237, p. 110993, 2024.

[15] T. Papadopoulos, Z. Datsios, A. Chrysochos, P. Mikropoulos, and G. Papagiannis, "Impact of the frequency-dependent soil electrical properties on the electromagnetic field propagation in underground cables," Proceedings of the International Conference on Power System Transients (IPST), Perpignan, France, 06 2019.

[16] H. Xue, A. Ametani, Y. Liu, and J. De Silva, "Effect of frequency-dependent soil parameters on wave propagation and transient behaviors of underground cables," International Journal of Electrical Power & Energy Systems, vol. 122, p. 106163, 2020.

[17] R. Tarko, J. Gajdzica, W. Nowak, and W. Szpyra, "Study of the lightning overvoltage protection effectiveness of high voltage mixed overhead cable power lines," Energies, vol. 14, no. 8, 2021.

[18] K. Velitsikakis and I. Tannemaat, "Insulation coordination for hvac cable sheath bonding systems in mixed ohl-ugc connections using the lightning statistics: A case study for the dutch 110 kv transmission grid," Electric Power Systems Research, vol. 223, p. 109654, 2023.

[19] A. Ametani, "A general formulation of impedance and admittance of cables," IEEE Transactions on Power Apparatus and Systems, vol. PAS-99, no. 3, pp. 902–910, 1980.

[20] R. Alipio and S. Visacro, "Modeling the frequency dependence of electrical parameters of soil," IEEE Transactions on Electromagnetic Compatibility, vol. 56, no. 5, pp. 1163–1171, 2014.

[21] Mission Research Corporation, "A universal impedance for soils," 735 State Street, Santa Barbara, California 93101, Tech. Rep., October 1975.

[22] D. Cavka, N. Mora, and F. Rachidi, "A comparison of frequency-dependent soil models: Application to the analysis of grounding systems," IEEE Transactions on Electromagnetic Compatibility, vol. 56, no. 1, pp. 177–187, 2013.

[23] T. A. Papadopoulos, Z. G. Datsios, A. I. Chrysochos, P. N. Mikropoulos, and G. K. Papagiannis, "Wave propagation characteristics and electromagnetic transient analysis of underground cable systems considering frequency-dependent soil properties," IEEE Transactions on Electromagnetic Compatibility, vol. 63, no. 1, pp. 259–267, 2021.

[24] A. G. Martins-Britto, T. A. Papadopoulos, Z. G. Datsios, A. I. Chrysochos, and G. K. Papagiannis, "Influence of lossy ground on high-frequency induced voltages on aboveground pipelines by nearby overhead transmission lines," IEEE Transactions on Electromagnetic Compatibility, vol. 64, no. 6, pp. 2273–2282, 2022.

[25] CIGRE Working Group C4.33, "Impact of soil-parameter frequency dependence on the response of grounding electrodes and on the lightning performance of electrical systems," p. 67, 2019.

[26] L. Wedepohl, "Application of matrix methods to the solution of travelling-wave phenomena in polyphase systems," Proceedings of the Institution of Electrical Engineers, vol. 110, pp. 2200–2212, 1963.

[27] L. Wedepohl, H. Nguyen, and G. Irwin, "Frequency-dependent transformation matrices for untransposed transmission lines using newton-raphson method," IEEE Transactions on Power Systems, vol. 11, no. 3, pp. 1538–1546, 1996.

[28] T. Nguyen and H. Chan, "Evaluation of modal transformation matrices for overhead transmission lines and underground cables by optimization method," IEEE Transactions on Power Delivery, vol. 17, no. 1, pp. 200–209, 2002.

[29] A. I. Chrysochos, T. A. Papadopoulos, and G. K. Papagiannis, "Robust calculation of frequency-dependent transmission-line transformation matrices using the levenberg–marquardt method," IEEE Transactions on Power Delivery, vol. 29, no. 4, pp. 1621–1629, 2014.

[30] A. G. Martins-Britto, T. A. Papadopoulos, and A. I. Chrysochos, "Transient electromagnetic interference between overhead and underground conductors," IEEE Transactions on Electromagnetic Compatibility, vol. 66, no. 3, pp. 983–992, 2024.

[31] CIGRE WG B1.30, "Cable Systems Electrical Characteristics," 2013, Technical Brochure 531.

[32] A. P. C. Magalhães, M. T. C. de Barros, and A. C. S. Lima, "Earth return admittance effect on underground cable system modeling," IEEE Transactions on Power Delivery, vol. 33, no. 2, pp. 662–670, 2018.

[33] P. Pettersson, "Propagation of waves on a wire above a lossy ground-different formulations with approximations," IEEE Transactions on Power Delivery, vol. 14, no. 3, pp. 1173–1180, 1999.

[34] J. E. Guevara, J. S. L. Colqui, and J. P. Filho, "Analysis of overvoltage and backflashover with different transmission line models," in SoutheastCon 2024, 2024, pp. 498–503.

[35] S. Visacro, A. Soares Jr., M. A. O. Schroeder, L. C. L. Cherchiglia, and V. J. de Sousa, "Statistical analysis of lightning current parameters: Measurements at morro do cachimbo station," Journal of Geophysical Research: Atmospheres, vol. 109, no. D1, 2004.

[36] F. H. Silveira and S. Visacro, "Lightning parameters of a tropical region for engineering application: Statistics of 51 flashes measured at morro do cachimbo and expressions for peak current distributions," IEEE Transactions on Electromagnetic Compatibility, vol. 62, no. 4, pp. 1186–1191, 2020.

[37] A. Xemard and E. Dorison, "Study of the protection of screen interruption joints against fast-front over-voltages," Proceedings of the International Conference on Power System Transients (IPST'05), 01 2005.